The Ferromagnetic Kondo Model for Manganites: Phase Diagram and Charge Segregation Effects.

E. Dagotto, S. Yunoki, A. L. Malvezzi, A. Moreo, and J. Hu
National High Magnetic Field Lab and Department of Physics,
Florida State University, Tallahassee, FL 32306

S. Capponi, and D. Poilblanc
Laboratoire de Physique Quantique Unité Mixte de Recherche 5626, C.N.R.S.,
Université Paul Sabatier, 31062 Toulouse, France

N. Furukawa
Institute for Solid State Physics,
University of Tokyo, Roppongi 7-22-1, Minato-ku, Tokyo 106, Japan

February 1, 2008

Abstract

The phase diagram of the ferromagnetic Kondo model for manganites is investigated using computational techniques. In clusters of dimensions 1 and 2, Monte Carlo simulations in the limit where the localized spins are classical show a rich low temperature phase diagram with three dominant regions: (i) a ferromagnetic phase, (ii) phase separation between hole-poor antiferromagnetic and hole-rich ferromagnetic domains, and (iii) a phase with incommensurate spin correlations. Possible experimental consequences of the regime of phase separation are discussed. Studies using the Lanczos algorithm and the Density Matrix Renormalization Group method applied to chains with localized spin 1/2 (with and without Coulombic repulsion for the mobile electrons) and spin 3/2 degrees of freedom give results in excellent agreement with those in the spin localized classical limit. The Dynamical Mean Field ($D = \infty$) approximation was also applied to the same model. At large Hund coupling phase separation and ferromagnetism were identified, again in good agreement with results in low dimensions. In addition, a Monte Carlo study of spin correlations allowed us to estimate the critical temperature for ferromagnetism T_c^{FM} in 3 dimensional clusters. It is concluded that T_c^{FM} is compatible with current experimental results.

1 Introduction and Main Results

Materials that present the phenomenon of "colossal" magnetoresistance are currently under much experimental investigation due to their potential technological applications. Typical compounds that have this phenomenon are ferromagnetic (FM) metallic oxides of the form $R_{1-x}X_xMnO_3$ (where $R = La, Pr, Nd$; $X = Sr, Ca, Ba, Pb$) [1, 2]. As an example, a decrease in resistivity of several orders of magnitude has been reported in thin films of $Nd_{0.7}Sr_{0.3}MnO_3$ at magnetic fields of 8 Teslas [3]. The relative changes in resistance for the manganites can be as large as $\Delta R/R \sim 100,000\%$, while in magnetic superlattices Co/Cu/Co the enhancement is about 100%. This result suggests that manganites indeed have technological potential since large changes in resistance can be obtained at fixed temperature upon the application of magnetic fields, opening an alternative route for next generation magnetic storage devices. However, since the development of La-manganite sensors is still at a very early stage, a more fundamental approach to the study of manganites is appropriate and, thus, theoretical guidance is needed. The existence of correlation effects in the fairly dramatic magnetic, transport, and magneto-transport properties of doped La-manganites reinforces this notion.

The early theoretical studies of models for manganites concentrated their efforts on the existence of ferromagnetism. The so-called "Double Exchange" (DE) model [4, 5] explained how carriers improve their kinetic energy by forcing the localized spins to become ferromagnetically ordered (this phenomenon is quite reminiscent of the Nagaoka phase discussed in models for cuprates). However, in spite of this successful explanation of the existence of ferromagnetism at low temperature several features of the experimental phase diagram of manganites remain unclear, and they are likely beyond the DE model.

Actually, the phase diagram of $La_{1-x}Ca_xMnO_3$ is very rich with not only ferromagnetic phases, but also regions with charge-ordering and antiferromagnetic correlations at $x > 0.5$ [6], and a poorly understood "normal" state above the critical temperature for ferromagnetism, T_c^{FM}, which has insulating characteristics at $x \sim 0.33$. Finding an insulator above T_c^{FM} is a surprising result since it would have been more natural to have a standard metallic phase in that regime which could smoothly become a ferromagnetic metal as the temperature is reduced. Some theories for manganites propose that the insulating regime above T_c^{FM} is caused by a strong correlation between electronic and phononic degrees of freedom [7]. Other proposals include the presence of Berry phases in the DE model that may lead to electronic localization [8]. On the other hand, the regime of charge ordering has received little theoretical attention and its features remain mostly unexplored. To complicate matters further, recent experiments testing the dynamical response of manganites have reported anomalous results in the ferromagnetic phase using neutron scattering [9], while in photoemission experiments [10] the possible existence of a pseudogap above the critical temperature was reported.

The rich phase diagram of the manganites described above, plus the several experimental indications of strong correlations in the system, deserves a systematic theoretical study using state-of-the-art computational techniques. These methods are unbiased and can provide useful information on models for manganites in a regime of couplings that cannot be handled perturbatively or exactly. However, the large number of degrees of freedom and associated couplings of a full Hamiltonian model for manganites makes this approach quite cumbersome. In principle the two e_g active orbitals per Mn-ion must be included, in addition to the t_{2g} electrons. Also phonons should be incorporated to fully describe these materials. However, as a first step towards a theoretical understanding of the behavior of models for manganites, in this paper it was decided to work only in the electronic sector (i.e. leaving aside phonons) and with just one orbital per site (i.e. keeping only one e_g orbital of the two available, which in practice amounts to assuming a static Jahn-Teller distortion). In addition, the t_{2g} degrees of freedom are here assumed to be localized i.e. no mobility is given to these electrons. They basically provide a spin background in which the e_g electrons move, with a Hund term that couples all active electrons per Mn-ion. Under these assumptions a rich phase diagram was obtained, as explained in detail in the rest of the paper. It is left for future work the analysis of the influence of phonons and orbital degeneracy into the fairly complicated phase diagrams reported here.

Some of the main results of the present effort are summarized in Figs.1 and 2 where the phase diagrams of the ferromagnetic Kondo model, using classical spins to represent the t_{2g} spins, are presented for low dimensional systems. These figures were reported previously in a short version of this paper [11] but here considerable more details, as well as a large set of novel results, are provided. Three dominant regimes have been identified: (1) a ferromagnetic region in excellent agreement with the DE mechanism, (2) phase separation between hole-rich ferromagnetic and hole-poor antiferromagnetic regions, and (3) an intermediate phase with short-range incommensurate correlations. The regime of phase separation was previously conjectured to exist in this model from studies of Hamiltonians for manganites at large Hund coupling in one dimension [12]. It is important to remark that phase separation is currently widely discussed in the context of high temperature superconductors since models for the cuprates, such as the $t-J$ model in two dimensions, present densities that cannot be uniformly stabilized in a given volume by suitably selecting a chemical potential [13, 14, 15]. After the introduction of $1/r$ Coulombic interactions the resulting hole-rich regions become unstable against the formation of "stripe" configurations [16, 17]. If the tendencies towards phase separation reported in this paper are realized in the manganites, a similar phenomenon may likely occur i.e. neutron scattering experiments could reveal evidence of stripe configurations in compounds such as $La_{1-x}Ca_xMnO_3$ as it occurs in the cuprates [18]. The pseudogap features found in photoemission [10] could also be related to this phenomenon.

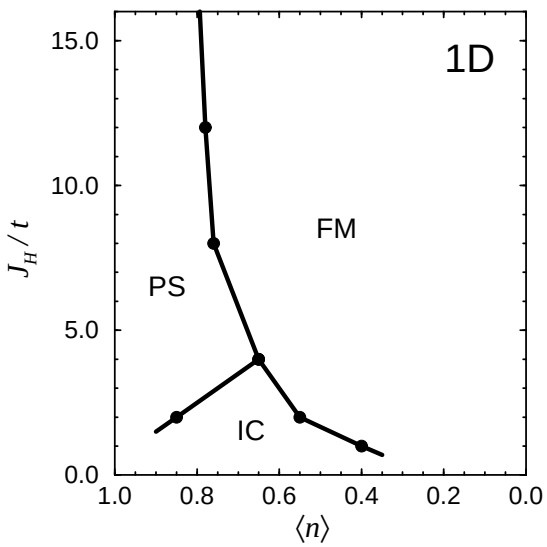

Figure 1: Phase diagram of the ferromagnetic Kondo model in one dimension obtained with Monte Carlo techniques in the limit where the localized spins are classical. PS, FM, and IC denote regions with phase separation, ferromagnetism, and incommensurate correlations. For details see the text.

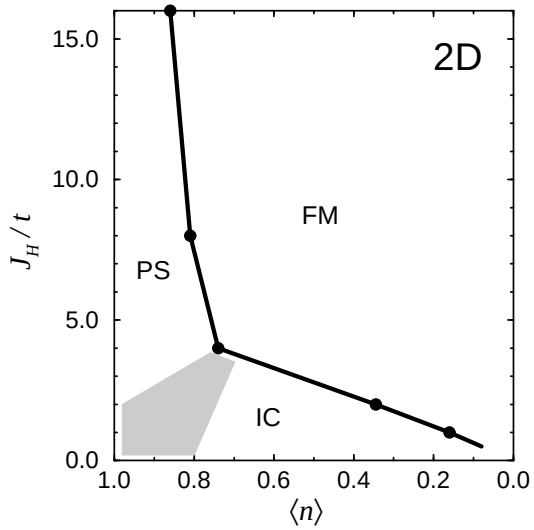

Figure 2: Same as Fig.1 but for the case of two dimensions. The boundary between the PS and IC regimes was difficult to obtain numerically and, thus, it is not sharply defined in the figure (gray region).

The bulk of the paper is devoted to the discussion of the numerical evidence that provides support to these proposed phase diagrams. Results were not only obtained in dimensions 1 (Secs.III and IV) and 2 (Sec.V), but also in 3 (Sec.VII) and ∞ (Sec.VI) using a variety of numerical techniques. Both classical and quantum mechanical t_{2g} degrees of freedom were analyzed on chains. Experimental consequences of our results are discussed, specially those related with the existence of phase separation (Sec.VIII). There is a clear underlying qualitative universality between results obtained on lattices with different coordination number and using different algorithms. This universality lead us to believe that the results reported here contain at least the dominant main features of the phase diagram corresponding to realistic electronic models for manganites that have been widely discussed before in the literature, but which were not systematically studied using computational methods.

2 Model, Symmetries and Algorithm

The ferromagnetic Kondo Hamiltonian [4, 19] studied in this paper is defined as

$$H = -t \sum_{\langle \mathbf{ij} \rangle \sigma} (c^\dagger_{\mathbf{i}\sigma} c_{\mathbf{j}\sigma} + h.c.) - J_H \sum_{\mathbf{i}\alpha\beta} c^\dagger_{\mathbf{i}\alpha} \sigma_{\alpha\beta} c_{\mathbf{i}\beta} \cdot \mathbf{S_i}, \quad (1)$$

where $c_{\mathbf{i}\sigma}$ are destruction operators for electrons at site $\mathbf{i}$ with spin σ, and $\mathbf{S_i}$ is the total spin of the t_{2g} electrons, assumed localized. The first term is the electron transfer between nearest-neighbor Mn-ions, $J_H > 0$ is the ferromagnetic Hund coupling, the number of sites is L, and the rest of the notation is standard. The boundary conditions used in the present study are important for some results, and they will be discussed later in the text. The electronic density of e_g electrons, denoted by $\langle n \rangle$, is adjusted using a chemical potential μ. In several of the results shown below the spin $\mathbf{S_i}$ will be considered classical (with $|\mathbf{S_i}| = 1$). In 1D both classical and quantum mechanical t_{2g} spins will be studied, the latter having a realistic spin 3/2 but also considering spin 1/2 for comparison. Phenomenologically $J_H \gg t$, but here J_H/t was considered an arbitrary parameter, i.e. both large and small values for J_H/t were studied. Below some calculations were also carried out including a large on-site Coulombic repulsion among the mobile electrons.

For a one-dimensional chain (open ends), or for a one-dimensional ring with L even and periodic or antiperiodic boundary conditions (PBC and APBC, respectively) the model is particle-hole symmetric with respect to $\langle n \rangle = 1$ by simply transforming $c^\dagger_{\mathbf{i}\uparrow} \rightarrow (-1)^{\mathbf{i}} c_{\mathbf{i}\downarrow}$ and $c^\dagger_{\mathbf{i}\downarrow} \rightarrow -(-1)^{\mathbf{i}} c_{\mathbf{i}\uparrow}$ for the mobile electrons. In this case the density is transformed as $\langle n \rangle \rightarrow 2 - \langle n \rangle$. Similar transformations can be deduced for clusters of dimension larger than one. Then, here it is sufficient to study densities $\langle n \rangle \leq 1$.

The FM Kondo model Eq.(1) with classical spins can be substantially simplified if the limit $J_H \rightarrow \infty$ is also considered. In this situation at every site only the spin component of the mobile electrons which is parallel to the classical spin is a relevant degree of freedom. The best way to make this reduction in the Hilbert space is by rotating the $c_{\mathbf{i}\sigma}$ operators into new operators $d_{\mathbf{i}\alpha}$ using a 2×2 rotation matrix such that the transformed spinors point in the direction of the classical spin. Explicitly, the actual transformation is:

$$c_{\mathbf{i}\uparrow} = \cos(\theta_{\mathbf{i}}/2)\ d_{\mathbf{i}\uparrow} - \sin(\theta_{\mathbf{i}}/2) e^{-i\phi_{\mathbf{i}}}\ d_{\mathbf{i}\downarrow}, \quad (2.1)$$

$$c_{\mathbf{i}\downarrow} = \sin(\theta_{\mathbf{i}}/2) e^{i\phi_{\mathbf{i}}}\ d_{\mathbf{i}\uparrow} + \cos(\theta_{\mathbf{i}}/2)\ d_{\mathbf{i}\downarrow}. \quad (2.2)$$

The angles $\theta_{\mathbf{i}}$ and $\phi_{\mathbf{i}}$ define the direction of the classical spin at site $\mathbf{i}$. After this transformation the new Hamiltonian becomes

$$H_{J_H=\infty} = -\sum_{\langle \mathbf{m},\mathbf{n} \rangle} (t_{\mathbf{m},\mathbf{n}} d^\dagger_{\mathbf{m}\uparrow} d_{\mathbf{n}\uparrow} + h.c.), \quad (3)$$

where the down component of the new operators has been discarded since the $J_H \rightarrow \infty$ limit is considered. The effective hopping is

$$t_{\mathbf{m},\mathbf{n}} = t\,[\cos(\theta_{\mathbf{m}}/2)\cos(\theta_{\mathbf{n}}/2) + \sin(\theta_{\mathbf{m}}/2)\sin(\theta_{\mathbf{n}}/2) e^{-i(\phi_{\mathbf{m}}-\phi_{\mathbf{n}})}], \quad (4)$$

i.e. it is complex and dependent on the direction of the classical spins at sites $\mathbf{m}, \mathbf{n}$ [8]. In the limit $J_H = \infty$ the band for the transformed spinors with up spin has itself a particle-hole symmetry, which exists for any arbitrary configuration of classical spins. This can be shown by transforming $d^\dagger_{\mathbf{i}\uparrow} \rightarrow (-1)^{\mathbf{i}} d_{\mathbf{i}\uparrow}$, and noticing that after this transformation the resulting Hamiltonian matrix is simply the conjugate of the original. Then, the eigenvalues are unchanged, but $\langle d^\dagger_{\mathbf{i}\uparrow} d_{\mathbf{i}\uparrow} \rangle \rightarrow 1 - \langle d^\dagger_{\mathbf{i}\uparrow} d_{\mathbf{i}\uparrow} \rangle$.

The partition function of the FM Kondo model with classical spins can be written as

$$Z = \prod_{\mathbf{i}}^{L} \left(\int_0^\pi d\theta_{\mathbf{i}} \sin\theta_{\mathbf{i}} \int_0^{2\pi} d\phi_{\mathbf{i}} \right) \mathrm{tr}_c(e^{-\beta H}). \quad (5)$$

For a fixed configuration of angles $\{\theta_{\mathbf{i}}, \phi_{\mathbf{i}}\}$ the Hamiltonian amounts to non-interacting electrons moving in an external field. This problem can be diagonalized exactly since the Hamiltonian is quadratic in the fermionic variables. This diagonalization is performed simply by calling a library subroutine in a computer program. If the $2L$ eigenvalues are denoted by ϵ_λ the resulting partition function becomes

$$Z = \prod_{\mathbf{i}}^{L} \left(\int_0^\pi d\theta_{\mathbf{i}} \sin\theta_{\mathbf{i}} \int_0^{2\pi} d\phi_{\mathbf{i}} \right) \prod_{\lambda=1}^{2L} (1 + e^{-\beta\epsilon_\lambda}). \quad (6)$$

The integrand in Eq.(6) is positive and, thus, a Monte Carlo simulation can be performed on the classical spin angles without "sign" problems. This was the procedure followed in our study below. The number of sweeps through the lattice needed to obtain good statistics varied widely depending on the temperature, densities, and couplings. In some cases, such as in the vicinity of phase separation regimes, up to 10^6 sweeps were needed to collect good statistics. Measurements of equal-time spin and charge correlations for the mobile electrons were performed by transforming the operators involved using the basis that diagonalizes the Hamiltonian for a fixed configuration of classical spins. Dynamical studies of the optical conductivity $\sigma(\omega)$ and the one particle spectral function $A(\mathbf{p}, \omega)$ could also be performed following a similar procedure, but their detailed study is postponed for a future publication. The analysis of the FM Kondo model in the case of quantum mechanical t_{2g} degrees of freedom was performed at zero temperature using standard Lanczos [14, 20] and Density Matrix Renormalization Group (DMRG) [21] techniques. The study at infinite dimension was carried out with the Dynamical Mean-Field approach [19].

3 Results in D=1 with Classical Localized Spins

In this section the computational results that led us to propose Fig.1 as the phase diagram of the FM Kondo model in one dimension using classical spins are presented. Results for quantum mechanical t_{2g} spins are also provided.

3.1 Ferromagnetism

The boundary of the ferromagnetic region in Fig.1 was obtained by studying the spin-spin correlations (between the classical spins) defined in momentum space as $S(q) = (1/L) \sum_{j,m} e^{i(j-m)\cdot q} \langle \mathbf{S}_j \cdot \mathbf{S}_m \rangle$, using a standard notation, at the particular value of zero momentum. L is the number of sites. The analysis was performed for couplings $J_H/t = 1, 2, 3, 4, 8, 12$ and 18. For the last four (strong) couplings and in the region of densities that were found to be stable (see next section for a discussion) the real space spin-spin correlations $\langle \mathbf{S}_j \cdot \mathbf{S}_m \rangle$ have a robust tail that extends to the largest distances available on the clusters studied here. This is obviously correlated with the presence of a large peak in $S(q)$ at zero momentum. Fig.3 shows representative results at $J_H/t = 12$ using open boundary conditions (OBC) and $L = 24$. A robust ferromagnetic correlation is clearly observed even at large distances. The strength of the tail decreases as $\langle n \rangle$ increases in the region $\langle n \rangle \geq 0.5$, and it tends to vanish at a density ~ 0.78 which corresponds to the boundary of the ferromagnetic region in Fig.1. A similar behavior is observed for smaller values of the coupling. It is interesting to note that the maximum strength of the spin-spin correlation tail appears at $\langle n \rangle \approx 0.50$. This result is compatible with the behavior expected at $J_H = \infty$ where large and small densities are exactly related by symmetry (as discussed in Sec.II) and, thus, the ferromagnetic correlations should peak at exactly $\langle n \rangle = 0.50$. Working at $J_H/t \leq 8$ this qualitative behavior is washed out and in this regime the correlations at densities $\langle n \rangle \leq 0.50$ are very similar.

Special care must be taken with the boundary conditions (BC). Closed shell BC or open BC are needed to stabilize a ferromagnetic spin arrangement. If other BC are used the spin correlations at short distances are still strongly FM (if working at couplings where ferromagnetism is dominant), but not at large distances where they become negative since a kink appears separating two regions of opposite total spin, with each region having all spins aligned in the same direction. This well-known effect was observed before in a similar context [12, 22] and it does not present a problem in the analysis shown below. Actually results using other boundary conditions and lattice lengths up to 60 sites are compatible with the data of Fig.3. In particular it can be shown that the ferromagnetic correlations persist when the lattice size is increased. Fig.4a shows $S(q = 0)$ versus temperature for several lattice sizes. At small temperature the sum over sites of the correlations grow with L showing that the FM correlation length is larger than the size of the chains used here. However, in 1D the Mermin-Wagner theorem forbids the existence of a finite critical temperature and, thus, eventually $S(q = 0)$ must tend to saturate at any fixed finite temper-

ature T as L increases, as it already occurs for $T \geq 0.02$ in Fig.4a. In spite of this subtle detail, using closed-shell boundary conditions the numerical data presented in this subsection supports the presence of strong ferromagnetic correlations in the one dimensional FM Kondo model, and it is reasonable to expect that at zero temperature the model in the bulk will develop a finite magnetization in the ground state. Fig.4b contains the spin-spin correla-

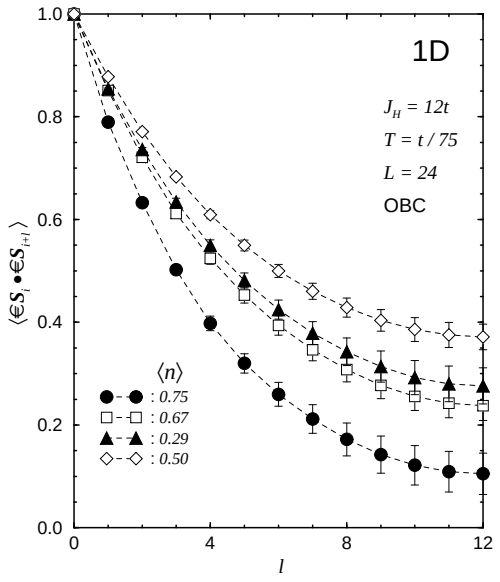

Figure 3: Spin-spin correlations among the localized spins (assumed classical) obtained with the Monte Carlo method working on a 1D system, and at the coupling, temperature, densities, and lattice size shown. Open boundary conditions were used. Clear strong ferromagnetic correlations are observed.

tions vs distance parametric with temperature. They show that even at relatively high temperatures, the correlations at *short* distances are clearly ferromagnetic, an effect that should influence on transport properties since carriers will react mainly to the local environment in which they are immersed. Fig.5 contains information that illustrates the formation of ferromagnetic spin polarons at relatively high temperatures. Fig.5a shows the spin correlations at low electronic density. At $T = t/10$ and distance 1, the correlation is only about 15% of the maximum. However, if this correlation is measured in the immediate vicinity of a carrier using $\langle n_i^e \mathbf{S}_i \cdot \mathbf{S}_{i+l} \rangle$, where $n_i^e = \sum_\sigma n_{i\sigma}(1 - n_{i-\sigma})$ and $n_{i\sigma}$ is the number operator for e_g-electrons at site i and with spin projection σ, then the correlation is enhanced to 40%. Thus, it is clear that FM correlations develop in the vicinity of the carrier [23]. This spin polaron apparently has a size of 3 to 4 lattice spacings in our studies.

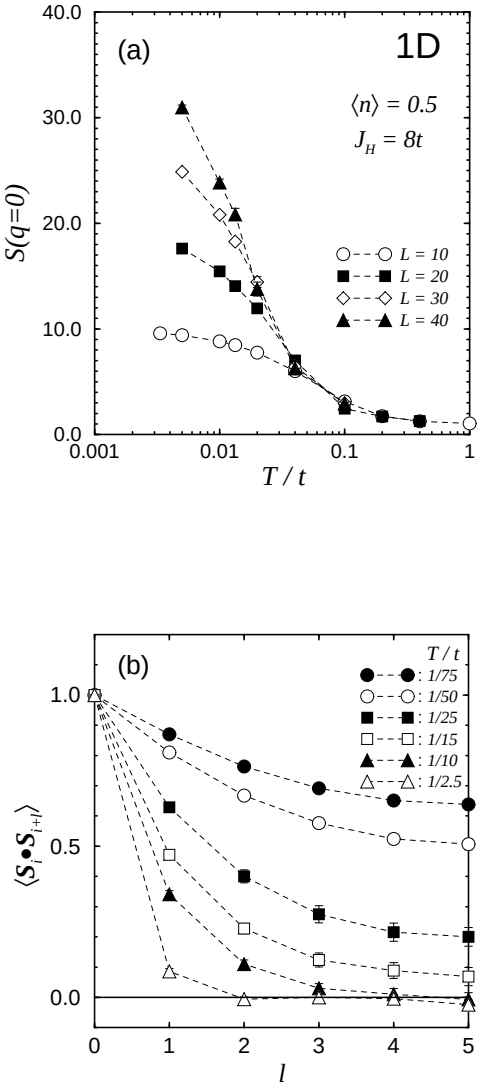

Figure 4: (a) Temperature dependence of the spin correlations in the one dimensional FM Kondo model using classical spins and the Monte Carlo method. Shown is the zero momentum spin structure factor $S(q)$ (for the classical spins) at the density, coupling, and lattice sizes indicated. Closed shell boundary conditions were used (periodic boundary conditions (PBC) for $L = 10$ and 30, and antiperiodic boundary conditions (APBC) for $L = 20$ and 40); (b) Spin-spin correlations at density $\langle n \rangle = 0.7$, using a 10 site chain, PBC, and $J_H/t = 8.0$. The temperatures are indicated.

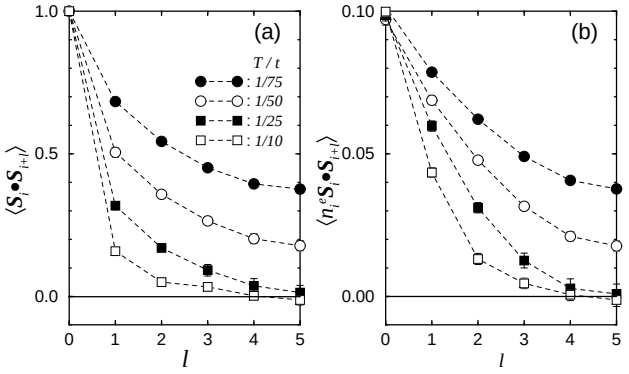

Figure 5: (a) Spin-spin correlations at $\langle n \rangle = 0.1$ using a chain of 10 sites with PBC. The Hund coupling is $J_H/t = 8.0$; (b) Similar as (a) but measuring the spin correlations near a conduction electron using $\langle n_i^e \mathbf{S}_i \cdot \mathbf{S}_{i+l} \rangle$, where n_i^e is defined in the text.

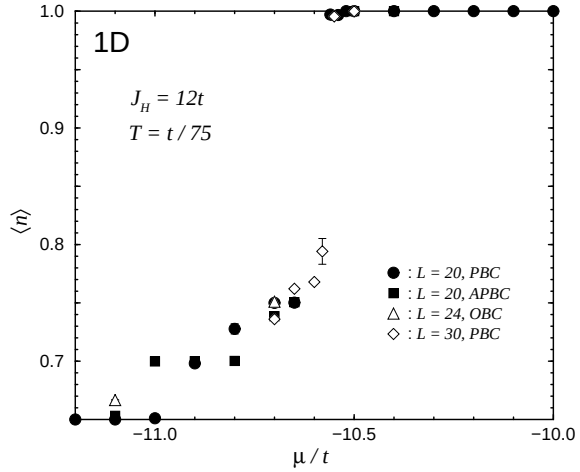

Figure 6: Electronic density $\langle n \rangle$ vs the chemical potential μ obtained with the Monte Carlo technique applied to the one dimensional FM Kondo model with classical spins. Coupling, temperature, lattice sizes, and boundary conditions are indicated. The discontinuity suggests that some densities are unstable, signaling the presence of phase separation.

3.2 Phase Separation

One of the main purposes of this paper is to report the existence of phase separation in the FM Kondo model. To study this phenomenon in the grand-canonical ensemble, where the Monte Carlo simulations are performed, it is convenient to analyze $\langle n \rangle$ versus μ. If $\langle n \rangle(\mu)$ is discontinuous then there are densities that can not be estabilized, regardless of the value of μ. The results shown in Fig.6 obtained at $J_H/t = 12$ clearly show that indeed phase separation occurs in the FM Kondo model. The discontinuity is between a density corresponding to the antiferromagnetic regime $\langle n \rangle = 1.0$ and ~ 0.77 where ferromagnetic correlations start developing, as shown before in Fig.3. In the case of the canonical ensemble these results can be rephrased as follows: if the system is initially setup with a density in the forbidden band, it will spontaneously separate into two regions having (i) antiferromagnetic (AF) correlations and no holes, and (ii) FM correlations and most of the holes.

The existence of phase separation can also be deduced from the actual Monte Carlo runs since they require large amounts of CPU time for convergence in the vicinity of the critical chemical potential μ_c. The reason is that in this regime there are two states in strong competition. Qualitatively this effect can be visualized analyzing $\langle n \rangle$ as a function of Monte Carlo time. Fig.7 shows such a time evolution when the chemical potential is fine tuned to its critical value $\mu_c \sim -6.69812t$ at $J_H/t = 8$. Wild fluctuations in $\langle n \rangle$ are observed with frequent tunneling events covering a large range of densities. A change in μ as small as 0.001 or even smaller reduces drastically the frequency of the tunneling events, and makes the results

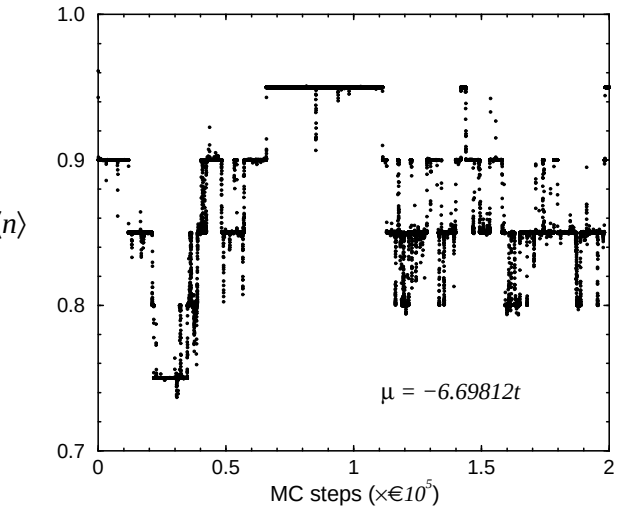

Figure 7: Monte Carlo time evolution of the density $\langle n \rangle$ at the particular value of μ where the discontinuity takes place working at $J_H/t = 8$, $T = t/75$, using $L = 20$ sites, and PBC. Frequent tunneling events are observed showing the competition between two states as in a first order phase transition.

more stable although certainly strong fluctuations remain in a finite window near μ_c. Fig.8 illustrates this effect showing a histogram that counts the number of times that

a density in a given window of density is reached in the simulation. As μ crosses its critical value the histograms change rapidly from having a large peak close to $\langle n \rangle \sim 1$ to a large peak at $\langle n \rangle \sim 0.75$. At densities that are stable away from the phase separation region these histograms present just one robust peak.

The qualitative behavior exemplified in Fig.6 was also observed at other values of J_H/t. For instance, Fig.9a contains resuls for $J_H/t = 4$ which are very similar to those found at a larger coupling. In a weaker coupling regime the discontinuity is reduced and now the competition is between the AF state and a state with incommensurate correlations rather than ferromagnetism. As example, Fig.9b contains results for $J_H/t = 2$. The discontinuity is located near $\mu_c \sim -1.35t$ and the two states competing in this regime actually have very similar properties. Analyzing, for instance, just $S(q)$ would have not provided an indication of a sharp discontinuity in the density, unlike the case of a large Hund coupling where the peak in the spin structure factor jumps rapidly from $q = \pi$ to 0 at the critical chemical potential.

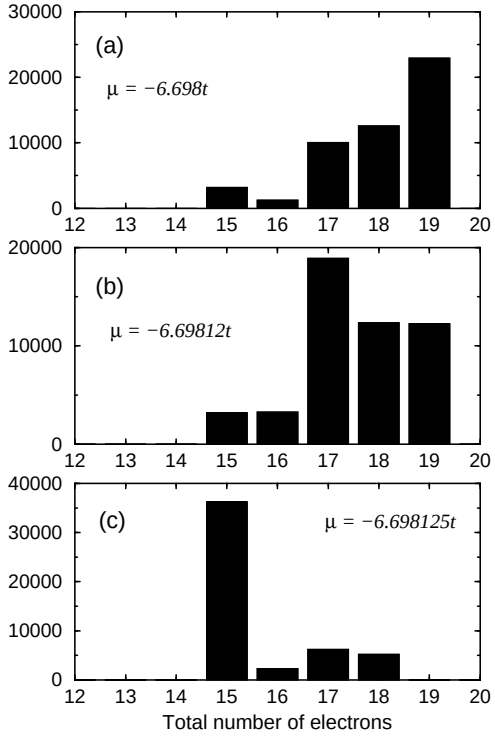

Figure 8: Hystogram for the total number of electrons obtained at $J_H/t = 8$, $T = t/75$, using periodic boundary conditions on a 20 sites chain. The chemical potentials are shown. (a) corresponds to a case where the average density is close to $\langle n \rangle = 1$, (b) is at the critical chemical potential, and at (c) the electronic density is close to 0.77.

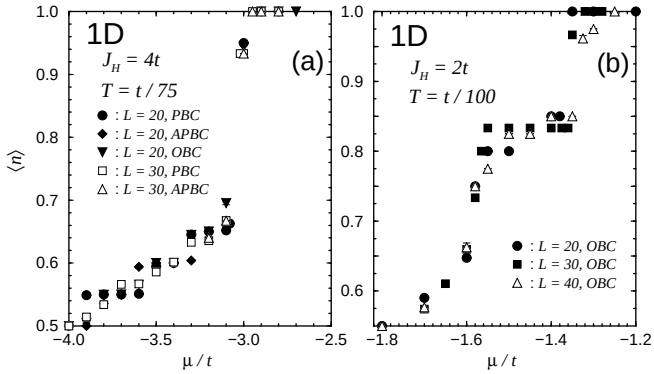

Figure 9: Electronic density vs μ for the FM Kondo model with classical spins in one dimension using Monte Carlo methods. A clear discontinuity signals the existence of phase separation. (a) corresponds to $J_H/t = 4$, while (b) is for $J_H/t = 2$. Temperatures, chain sizes, and boundary conditions are indicated. The apparent second discontinuity located at $\mu/t \sim -1.55$ in (b) is expected to be just a rapid crossover.

3.3 Incommensurate Correlations

The tendency to develop a spin pattern with incommensurate characteristics can be easily studied in our calculations observing the behavior of $S(q)$ as couplings and densities are varied. While at large J_H/t the spin structure factor is peaked only at the momenta compatible with ferro or antiferromagnetic order, a different result is obtained as J_H/t is reduced. Fig.10 shows $S(q)$ at $J_H/t = 1.0$ for a variety of densities. The AF peak close to $\langle n \rangle = 1$ smoothly evolves into a substantially weaker peak which moves away from $q = \pi$ in the range $0.5 \leq \langle n \rangle \leq 1.0$. The peak position is close to $2k_F = \langle n \rangle$, and since the spin-spin correlations for the mobile electrons show a similar behavior this is compatible with Luttinger liquids predictions [24]. In this density range, and for the lattice sizes and temperatures used here, the peak in $S(q)$ is broad and, thus, it cannot be taken as an indication of long-range incommensurate (IC) correlations but rather of the presence of IC spin arrangements at short distances. In the region of low densities $\langle n \rangle \leq 0.4$, $S(q)$ is now peaked at zero momentum which is compatible with the presence of robust ferromagnetic spin-spin correlations at the largest distances available in the studied clusters. The transition from one regime to the other in the intermediate small window $0.4 \leq \langle n \rangle \leq 0.5$ is very fast and was not studied in detail here, but for a second order phase transition it is expected to be continuous. In Fig.11 results for a slightly larger coupling $J_H/t = 2$ are shown. Here the pattern is more complicated since apparently the AF peak does

not evolve smoothly into the peak at $q \sim \pi/2$ observed at $\langle n \rangle = 0.733$, suggesting an interesting interplay between spin and charge.

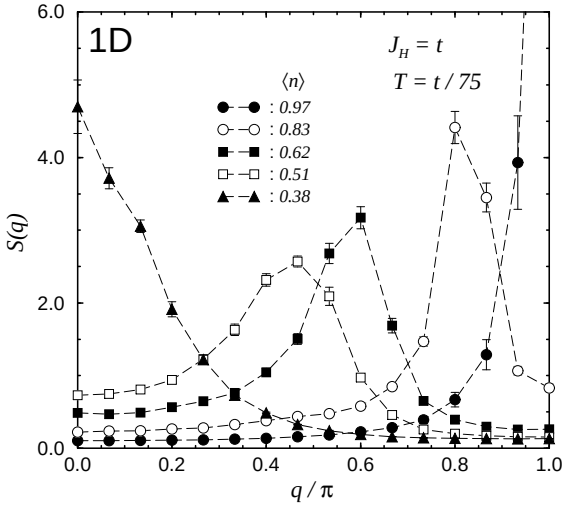

Figure 10: $S(q)$ (Fourier transform of the spin-spin correlations between classical spins) at $J_H = t$ and $T = t/75$, on a chain with 30 sites and PBC. The densities are indicated. The positions of the peaks indicate the tendency to have incommensurate correlations in the FM Kondo model.

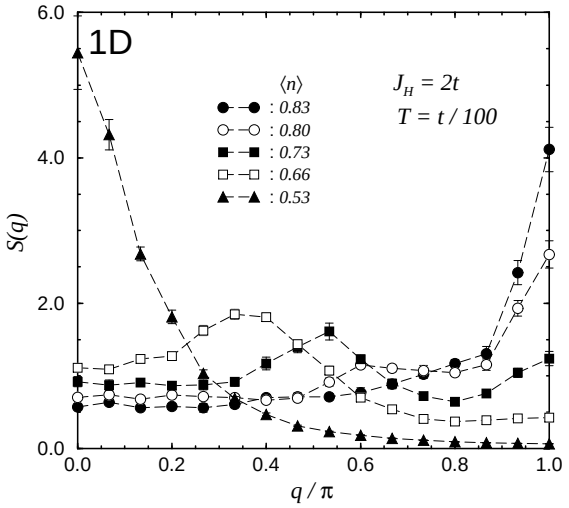

Figure 11: Same as Fig.10, but working at $J_H = 2t$ and $T = t/100$, with 30 sites and open boundary conditions (OBC).

Note that the presence of IC correlations in models for manganites was predicted theoretically using a Hartree-Fock approximation [25]. Our results are compatible with these predictions although, once again, it is not clear if the IC pattern corresponds to long-range order or simply short distance correlations. More work is needed to clarify these issues. Nevertheless, the present effort is enough to show that the tendency to form IC spin patterns exists in the FM Kondo model at small J_H/t.

3.4 Influence of a Direct Coupling Among the Localized Spins

The results of Sec.III.B show the presence of phase separation near half-filling, but not in the opposite extreme of low conduction electron density. This is a consequence of the absence of a direct coupling among the localized spins in Eq.(1). This coupling may be caused by a small hybridization between the t_{2g} electrons. If a Heisenberg term $J' \sum_{\langle ij \rangle} \mathbf{S}_i \cdot \mathbf{S}_i$ coupling the classical spins is added, then at $\langle n \rangle = 0$ an antiferromagnetic state is recovered similarly as at $\langle n \rangle = 1$. This term was already considered

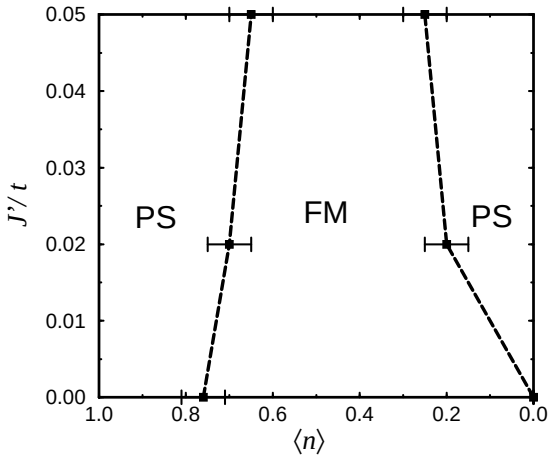

Figure 12: Phase diagram in the plane J'/t-$\langle n \rangle$ obtained studying the density vs μ calculated using the Monte Carlo technique with classical localized spins. The coupling is fixed to $J_H/t = 8$ and the temperature is low. Note that the regime of low density and $J'/t = 0$ is somewhat difficult to study due to the influence of van Hove singularities which produce a rapid change of the density with μ.

in the study of the strong coupling version of the Kondo model [12]. Although a detailed study of the influence of J' on the phase diagram Fig.1 is postponed for a future publication [26], here the effects of this new coupling into the existence of phase separation are reported. Following the same procedure described in Sec.III.B to obtain unstable densities, the phase diagram shown in Fig.12 was found. Note that at $J' \neq 0$ phase separation occurs at large *and*

small electronic densities. In the latter the separation is between electron-rich ferromagnetic and electron-poor antiferromagnetic regions. Then, the experimental search for phase separation discussed below in Sec.VIII should be carried out at both large and small hole densities. More details will be given elsewhere [26].

4 Results in D=1 with Quantum Localized Spins

4.1 Quantum Mechanical t_{2g} S=3/2 spins

The use of classical spins to represent the t_{2g} degrees of freedom is an approximation which has been used since the early days of the study of manganites [4, 5]. While such an approach seems reasonable it would be desirable to have some numerical evidence supporting the idea that using spin operators of value 3/2 (denoted by $\hat{\mathbf{S}}_\mathbf{i}$) the results are similar as those obtained with classical spins. Although numerical unbiased calculations with spins 3/2 are difficult in dimensions larger than 1, at least this issue can be addressed numerically with 1D chains using the Lanczos and Density Matrix Renormalization Group techniques. The Hamiltonian is the same as in Eq.(1) but now with quantum mechanical degrees of freedom normalized to 1 (i.e. replacing $\mathbf{S_i}$ by $\hat{\mathbf{S}}_\mathbf{i}/(3/2)$) to simplify the comparison of results against those obtained using classical spins. Calculating the ground state energy in subspaces with a fixed total spin in the z-direction, it is possible to study the tendency to have a ferromagnetic state in the model using the Lanczos technique. The results indicate that there is a robust region of fully saturated ferromagnetism, as indicated in Fig.13. The actual boundary of this region agrees accurately with the results obtained using classical spins shown in Fig.1. This reinforces the belief that S=3/2 and classical spins produce similar results, at least regarding ferromagnetism. Finite size effects are apparently small for the chains accessible with the DMRG method, as exemplified in Fig.14a where the ground state energy for $J_H/t = 6.0$ using a variety of chain lengths is presented.

To study other important features of the phase diagram, such as phase separation, the compressibility is needed. This quantity is defined as

$$\kappa^{-1} = \frac{N_e^2}{L} \frac{E(N_e+2,L) + E(N_e-2,L) - 2E(N_e,L)}{4}, \tag{7}$$

where $E(N_e, L)$ is the ground state energy corresponding to a chain with L sites and N_e electrons. If κ^{-1} becomes negative at some fixed density (remember that here the numerical study is in the canonical ensemble), the system is unstable and phase separation occurs. The DMRG results for the compressibility in Fig.14b for several couplings led us to conclude that the spin 3/2 model also has phase separation in the ground state near half-filling, simi-

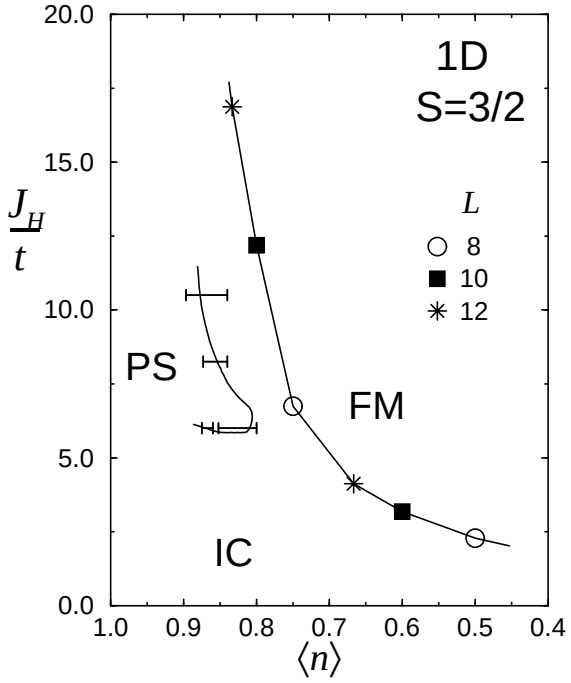

Figure 13: Phase diagram of the FM Kondo model with $S = 3/2$ localized t_{2g} spins obtained with the DMRG and Lanczos techniques applied to finite chains as indicated. The notation is as in Figs.1 and 2, i.e. ferromagnetism, incommensurability, and phase separation appear both for classical and quantum mechanical localized spins.

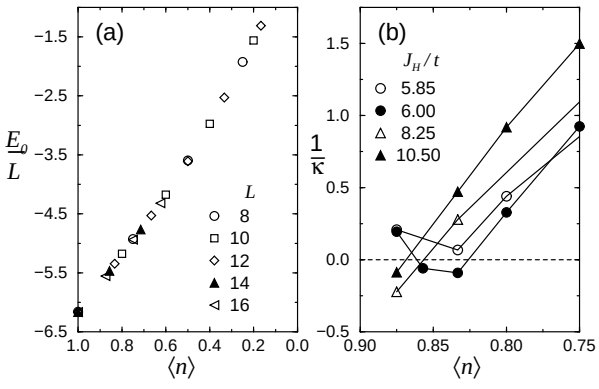

Figure 14: (a) Ground state energy per site vs density at $J_H/t = 6.0$ for the $S = 3/2$ FM Kondo model in 1D using DMRG techniques keeping $m = 48$ states. Results for a variety of chain lengths are shown; (b) Inverse compressibility vs density for the same model and chain lengths as in (a), calculated using several couplings. A negative $1/\kappa$ signals an unstable density.

larly as in the case of classical spins. Indeed Fig.14b shows that $1/\kappa$ becomes negative for densities in the vicinity of $\langle n \rangle \sim 0.85$ and larger, for the range of couplings shown. Thus, at least qualitatively there are tendencies to phase separate in the same region suggested by the simulations using classical localized spins.

However, a difference exists between results obtained with classical and quantum mechanical t_{2g} degrees of freedom: apparently there is a finite window in density between the phase separated and FM regimes in the phase diagram of Fig.13. This window could be a finite size effect, but the lack of a strong dependence with the chain lengths in the results of Fig.14a led us to believe that it may actually exist in the bulk limit. In addition, previous studies using the strong J_H/t coupling version of the FM Kondo model have also reported an intermediate window between phase separation and FM [12], and the analysis below for localized spins 1/2 suggests a similar result. Studying the spin of the ground state in this intermediate region here and in Ref.[12] it has been observed that it is $finite$ i.e. apparently partial ferromagnetism appears immediately at any finite stable density in the model with spins 3/2, at least working at intermediate and large Hund couplings [27]. The transition from phase separation to FM appears to be smooth in the spin quantum number, which is somewhat reminiscent of the results in the classical limit where the tail of the spin-spin correlation grows with continuity from small to large as the density diminishes in the stable region.

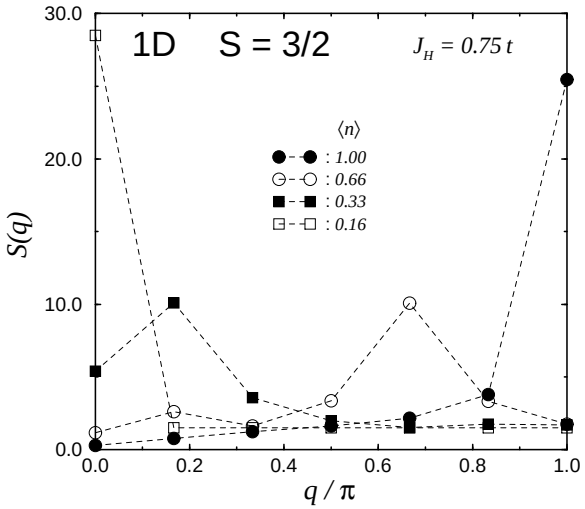

Figure 15: $S(q)$ for the quantum FM Kondo model using localized spins 3/2 on a chain of 12 sites. The technique is DMRG, keeping 48 states in the iterations. Densities and coupling are indicated. In the spin correlations used to obtain $S(q)$, full spins 3/2 (i.e. not normalized to 1) were used.

Finally, let us analyze whether incommensurate correlations exist in the spin 3/2 model as it occurs in the classical model. Fig.15 shows $S(q)$ obtained with DMRG working on a chain of 12 sites. Although momentum is not a good quantum number on a system with OBC, nevertheless using the same definition of the Fourier transform of the spin correlation as in the study of the classical system with periodic and antiperiodic boundary conditions (PBC and APBC, respectively), qualitative information about the tendency to form incommensurate structures can be gathered. The results of Fig.15 obtained at very small J_H/t indeed show that strong IC correlations exist in the ground state of this model, in agreement with the results of Figs.10 and 11 for classical spins. Then, it is concluded that the three dominant features of the phase diagram Fig.1 (PS, FM, and IC) have an analog in the case of the spin 3/2 quantum model. This agreement gives support to the believe that the results presented below in this paper for dimensions larger than one using classical spins should be qualitatively similar to those corresponding to a model with the proper quantum mechanical t_{2g} degrees of freedom.

4.2 Quantum Mechanical t_{2g} S=1/2 spins

For completeness, in this paper the special case of localized spins 1/2 in 1D has also been studied. The analysis has relevance not only in the context of manganites but also for recently synthesized one dimensional materials such as $Y_{2-x}Ca_xBaNiO_5$ which have a mobile and a localized electron per Ni-ion. This compound has been studied experimentally [28] and theoretically [29], and upon doping interesting properties have been observed including a metal-insulator transition. As discussed below, the conclusion of this subsection will be that the results for localized spins 1/2 are qualitatively similar to those obtained with classical and spin 3/2 degrees of freedom, i.e. ferromagnetism, incommensurability, and phase separation appear clearly in the phase diagram. The Hamiltonian used for this study is as defined in Eq.(1) but now with $\mathbf{S_i}$ replaced by a spin 1/2 operator (not normalized to 1). The technique used to obtain ground state properties is the finite-size DMRG method on chains with up to 40 sites, a variety of densities, and typical truncation errors around 10^{-5}. Some calculations were also performed with the Lanczos algorithm on lattices with up to 12 sites. The data obtained with the DMRG and Lanczos methods are qualitatively similar.

The main result is contained in the phase diagram shown in Fig.16. Three regimes were identified [30]. The region labeled FM corresponds to saturated ferromagnetism i.e. the ground state spin is the maximum. This regime was found using the Lanczos technique simply searching for degeneracies between the lowest energy states of subspaces with different total spin in the z-direction. For the IC regime, $S(q)$ was calculated using

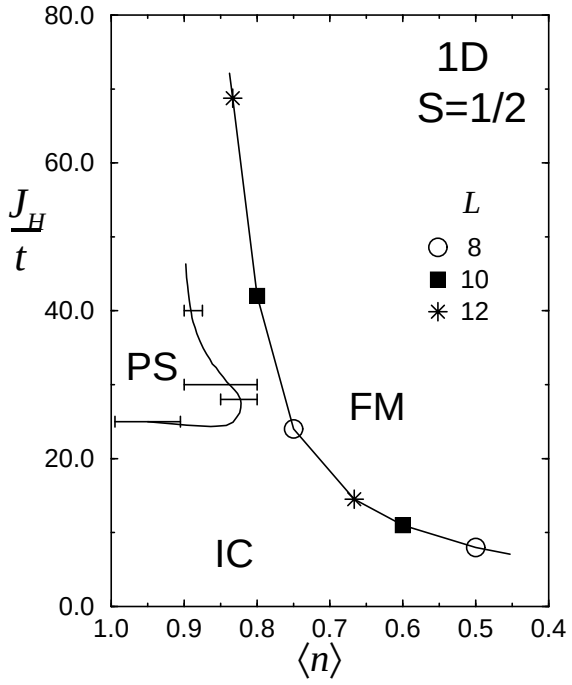

Figure 16: Phase diagram of the FM Kondo model with $S = 1/2$ localized states obtained with the DMRG and Lanczos methods. The length of the chains is indicated. The notation FM, PS, and IC is as in previous figures. Note the similarity with the results of Fig.13, up to an overall scale.

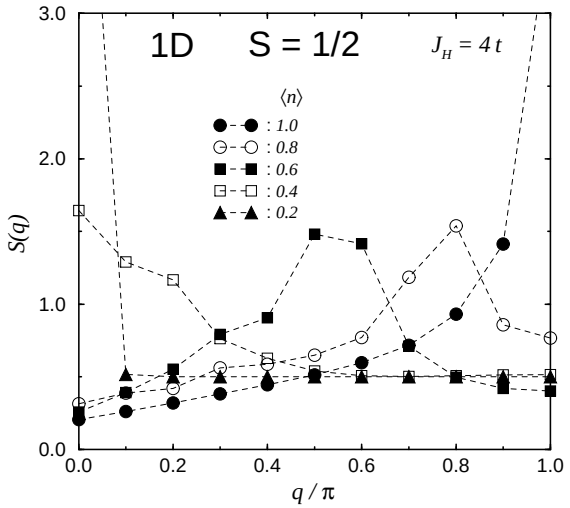

Figure 17: $S(q)$ for the quantum FM Kondo model using localized spins 1/2 on a chain of 20 sites. The technique is DMRG, keeping up to 60 states in the iterations. Densities and coupling are indicated. In the spin correlations used to obtain $S(q)$, full spins 1/2 (i.e. not normalized to 1) were used.

the same definition as in subsection III.A but now with spin 1/2 operators instead of classical spins of length 1. The results shown in Fig.17 suggest the presence of incommensurate correlations at small J_H/t, at least at short distances. Similarly as for the cases of larger localized spins (Figs.10 and 15), the peak in the spin structure factor moves smoothly from $q = \pi$ near $\langle n \rangle = 1$ to $q = 0$ in the FM region. The position of the peak is at $2k_F$. Our study also showed that correlated with this behavior the charge structure factor $N(q)$ has a cusp at the same position. It is important to clarify that in the IC regime of Fig.17 at low temperatures, the ground state has a finite spin but it is not fully saturated. Within the accuracy of our study the spin varies smoothly as the couplings and density are changed reaching its maximum value at the FM boundary.

The tendency to phase separate in this model can be studied calculating $\langle n \rangle$ vs μ. In the study of this section, carried out in the canonical ensemble where $\langle n \rangle$ is fixed, the procedure to obtain μ involves (i) the calculation of the ground state energy for a variety of densities, and (ii) the addition of $-\mu \hat{N}$ to the Hamiltonian, where $\hat{N}$ is the total number operator. As μ varies, different density subspaces become the actual global ground state. If there are densities that cannot be stabilized for any value of μ, then such a result is compatible with phase separation in the model (for more details see Ref. [31]). Results are presented in Fig.18.a,b,c for a chain with 20 sites: at small $J_H/t = 1$ all densities are accessible tuning μ, and the curvature of the ground state energy E_{GS} vs $\langle n \rangle$ is positive. However, working at $J_H/t = 30$ the density $\langle n \rangle = 0.9$ becomes unstable, and now E_{GS} vs $\langle n \rangle$ has less curvature. Fig.18d shows again density vs chemical potential but now on a larger chain of 40 sites. Here densities between 1 and 0.8 are unstable, in agreement with Fig.18c. A similar method to calculate the region of phase separation is to evaluate the inverse compressibility since a negative value for this quantity indicates phase separation, as explained in Sec.IV.A. Using this procedure once again a region of $\kappa^{-1} < 0$ was identified signaling unstable densities in the system. From the combination of these type of analysis performed for several chains, the boundaries of phase separation were estimated as shown in Fig.16. Although the error bars are not negligible, the presence of phase separation is a robust feature of the calculation and it is in excellent agreement with the conclusions of previous sections. Then, irrespective of the actual value of the spin corresponding to the t_{2g} degrees of freedom the phase diagram presents universal features, specially robust ferromagnetism, unstable densities, and short-range incom-

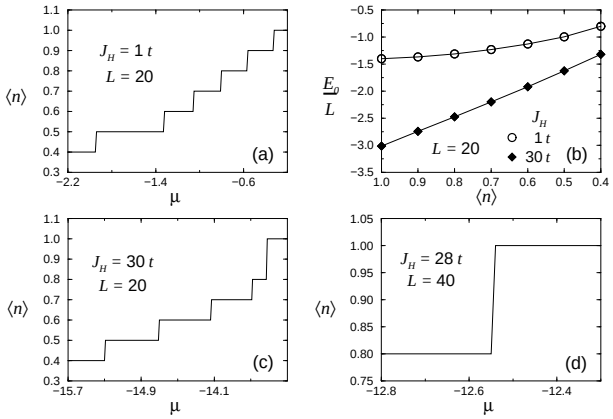

Figure 18: Results for the FM Kondo model with $S = 1/2$ localized spins using the DMRG method. (a) contains $\langle n \rangle$ vs μ for a chain of 20 sites at $J_H/t = 1$, showing that all available densities are accessible; (b) Ground state energy per site vs $\langle n \rangle$ for $J_H/t = 1$ and 30. The energies for the latter were divided by 5 to make both curves of comparable magnitude; (c) Same as (a) but for $J_H/t = 30$. Now $\langle n \rangle = 0.90$ appears unstable; (d) Results on a 40 sites chain at $J_H/t = 28$. The densities available between 1.00 and 0.80 (i.e. 0.95, 0.90, and 0.85) are unstable.

mensurate correlations. Below in Secs.V and VI, it will be shown that this universality can actually be extended to include higher dimensional clusters.

4.3 Influence of an On-site Coulomb Repulsion

The on-site Coulombic repulsion among electrons in the conduction band has been neglected thus far. Although it is not expected to produce qualitative changes in the physics described before (since a large J_H/t prevents double occupancy) it would be desirable to have some indications of its quantitative influence on the phase diagrams discussed in previous sections. Unfortunately, the addition of a Hubbard repulsion U complicates substantially the many-body numerical studies. The Monte Carlo method in the classical limit can only proceed after the Hubbard U-term is decoupled using Hubbard-Stratonovich (HS) variables. If such a procedure is followed the simulation would run over both angles and HS degrees of freedom, and likely a "sign" problem would occur. Such a cumbersome approach will not be pursued here. Instead the large U/t limit for the case of localized spins 1/2 will be investigated using the Lanczos method, which can be applied without major complications to the study of Hubbard-like systems. The study will be limited to chains due to restrictions on the size of the clusters that can be analyzed numerically. In addition, in the strong coupling limit the Hubbard model becomes the $t - J$ model, and, thus, the actual Hamiltonian studied here is defined as

$$H = J \sum_i [s_i \cdot s_{i+1} - (1/4) n_i n_{i+1}]$$

$$- t \sum_{i\sigma} (\hat{c}^\dagger_{i\sigma} \hat{c}_{i+1\sigma} + h.c.) - J_H \sum_i \mathbf{s}_i \cdot \mathbf{S}_i, \qquad (8)$$

where $\hat{c}$ is a destruction fermionic operators which includes a projector operator avoiding double occupancy. Both $\mathbf{S}_i$ and $\mathbf{s}_i$ are spin-1/2 operators representing the spin of the localized and mobile degrees of freedom, respectively. The rest of the notation is standard.

Once again studying the energy of the ground state for subspaces with different total spin projection in the z-direction, the existence of ferromagnetism can be studied. The boundary of the region with fully saturared ferromagnetism obtained using clusters with 8 and 10 sites is shown in Fig.19a. Strong ferromagnetic correlations appear even for small values for J_H/t, suggesting that as U/t grows the tendency to favor ferromagnetism increases, as noticed also in Ref. [12]. It is interesting to observe that in the region not labeled as FM in Fig.19a a finite spin exists in the ground state (see Fig.19b), in excellent agreement with results for the $U/t = 0$ case reported in Sec.IV.A and IV.B for quantum mechanical t_{2g} degrees of freedom (see also Ref.[12]). In addition, a tendency towards incommensurate correlations is observed in this phase, also in agreement with previous results (see Fig.19c). Regarding the issue of phase separation, the results of Fig.16 suggests that this regime should appear for densities between $\langle n \rangle = 1.0$ and $\langle n \rangle = 0.90$. Unfortunately these densities are not accessible on the clusters studied in this subsection, and, thus, the confirmation of the existence of phase separation at large U/t will still require further numerical work [32]. Nevertheless, Figs.16 and 19a, which contain results with and without the Coulomb interaction, have clear qualitative common trends. Regarding the quantitative aspects, the Coulomb interaction changes substantially the scales in the phase diagram specially regarding ferromagnetism which now appears at smaller values of J_H/t [33].

5 Results in D=2

In this section the computational results that led us to propose Fig.2 as the phase diagram of the FM Kondo model in two dimensions are presented. Results in 2D are particularly important since manganite compounds with layered structure have been recently synthesized [34].

5.1 Ferromagnetism

The search for ferromagnetism in the ground state of the 2D clusters was carried out similarly as in 1D for the case of classical t_{2g} spins. The real space spin-spin correlations

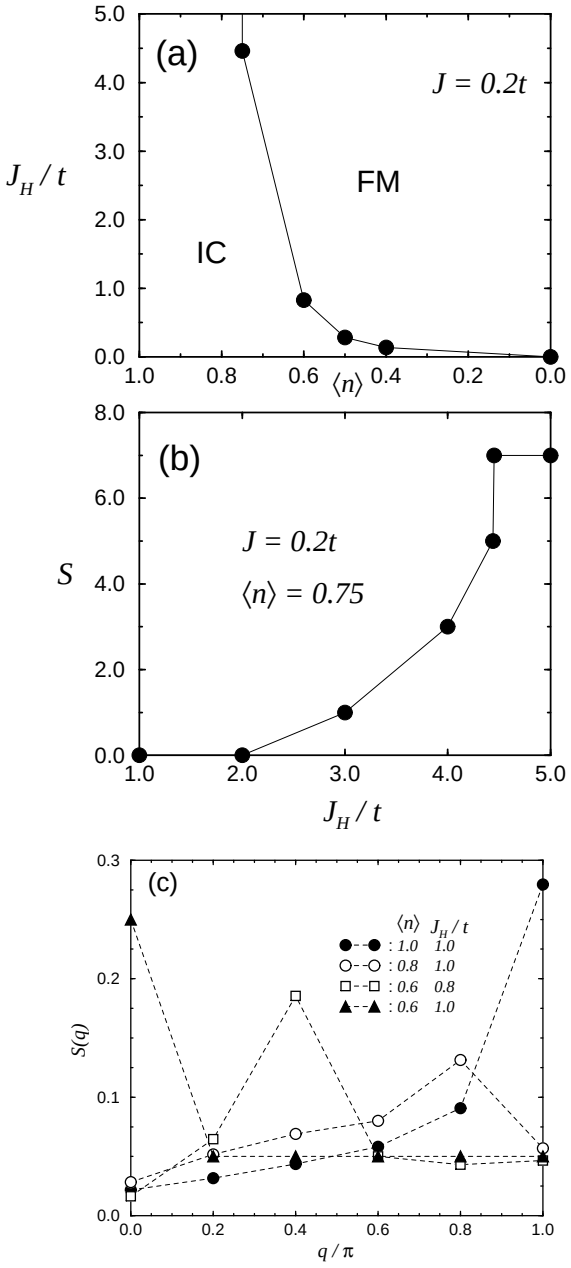

Figure 19: Results corresponding to the FM Kondo model with localized spins 1/2 and using the $t-J$ model for the mobile electrons (Eq.(8)), obtained with the Lanczos method. The boundary conditions were such that a fully saturared ferromagnetic states is stable. $J/t = 0.2$ was used. (a) shows the boundary of the FM region using 8 and 10 sites clusters. IC correlations were observed at small J_H/t in the non-fully saturated ferromagnetic region; (b) the spin of the ground state as a function of J_H for the case of 2 holes on the 8 sites cluster; and (c) $S(q)$, the Fourier transform of the spin-spin correlations between the localized spins, vs momentum for the case of a 10 sites cluster. The densities and couplings are indicated.

(between those classical spins) was monitored, as well as its Fourier transform $S(q)$ at zero momentum. Couplings $J_H/t = 1, 2, 4, 8$, and 16 were particularly analyzed. Typical results are presented in Fig.20 where the spin correlations are presented at a fixed coupling, parametric with the electronic density. It is clear that the tails of the correlations are very robust, and the ferromagnetic correlation length exceeds the maximum distance, d_{max}, available on the 6×6 cluster. Plotting the spin correlation at d_{max} vs $\langle n \rangle$, an estimate of the critical density for ferromagnetism can be obtained. Combining results from a variety of clusters and boundary conditions, the FM boundary of Fig.2 was constructed. Note that for this analysis the use of open boundary conditions seem to be the optimal i.e. using other boundary conditions kept the ferromagnetic character of the system at short distances but modify the correlations at large distances, as it occurs for non-closed-shell BC in 1D.

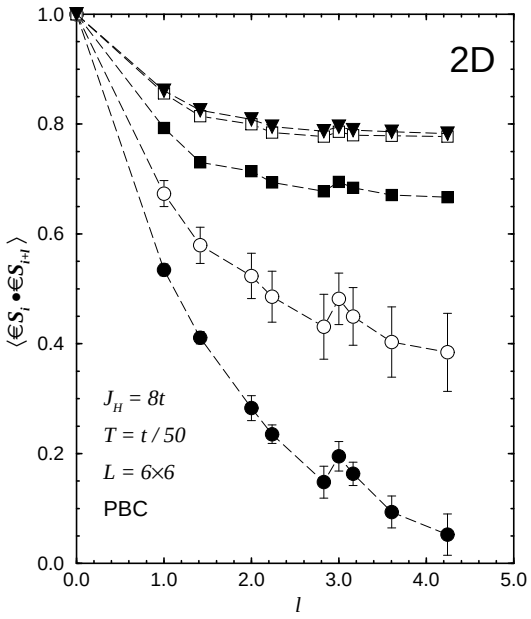

Figure 20: Spin-spin correlations (among the classical spins) vs. distance obtained at $J_H/t = 8$, $T = t/50$, and using periodic boundary conditions on a 6×6 cluster. Full circles, open circles, full squares, open squares, and full triangles correspond to densities $\langle n \rangle = 0.807$, 0.776, 0.750, 0.639, and 0.285, respectively.

The influence of the lattice size can be estimated by studying $S(q)$ vs temperature for several clusters. Representative results are shown in Fig.21. They were obtained at $J_H/t = 16$ and a density close to the PS-FM boundary. At low temperature $S(q = 0)$ clearly grows with the lattice size due to the strong ferromagnetic correlations.

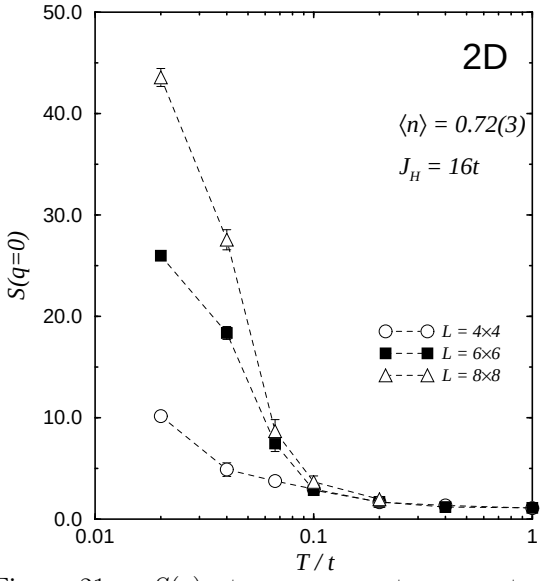

Figure 21: $S(q)$ at zero momentum vs. temperature, working at $\langle n \rangle = 0.72 \pm 0.03$, $J_H/t = 16$, using open boundary conditions, and for the two-dimensional cluster sizes shown.

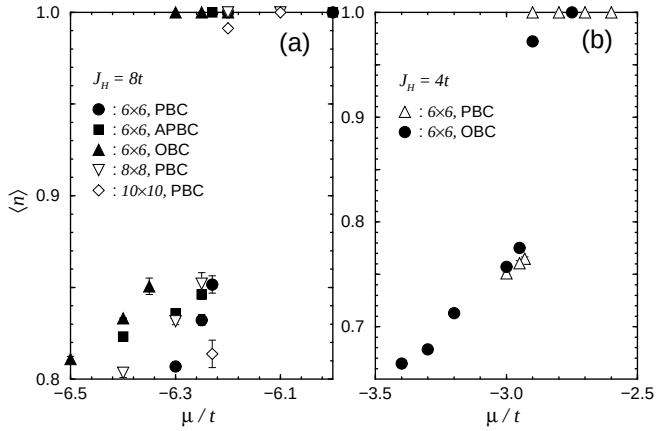

Figure 22: $\langle n \rangle$ vs μ on two-dimensional clusters and at temperature $T = t/50$, to illustrate the presence of phase separation in the 2D ferromagnetic Kondo model with classical spins. (a) contains results at $J_H/t = 8$ and a variety of clusters and boundary conditions. (b) corresponds to $J_H/t = 4$, a 6×6 cluster, and using both periodic and open boundary conditions.

However, as in the case of 1D, the Mermin-Wagner theorem forbids long-range ferromagnetism in 2D at finite temperature and, thus, $S(q)$ should converge to a finite constant if the lattice sizes are further increased beyond those currently accessible, working at a fixed finite temperature. The verification of this subtle detail is beyond the scope of this paper, and should not confuse the readers: the presence of very strong ferromagnetic correlations at low temperature in the FM Kondo model is clear in the present numerical study and it is likely that small couplings in the direction perpendicular to the planes would stabilize ferromagnetic order at a finite temperature.

5.2 Phase Separation

The computational analysis carried out in this subsection show that the phenomenon of phase separation occurs not only in one dimension but also in two dimensions (and higher). This result indicates that the unstable densities found in Secs.III and IV are not a pathology of 1D clusters but its existence is generic of the FM Kondo model.

Typical numerical results in 2D clusters at low temperature are shown in Fig.22a at $J_H = 8t$. Data from a variety of cluster sizes and boundary conditions are presented. Although the results corresponding to the lowest density in the discontinuity in $\langle n \rangle$ are somewhat scattered due to size effects, the existence of such discontinuity is clear from the figure. Fig.22b contains similar results but now for $J_H/t = 4$. Once again, $\langle n \rangle$ is discontinuous signaling the presence of phase separation in the low temperature regime of the FM Kondo model. Calculating the discontinuity in $\langle n \rangle$ for several couplings the boundary of the phase separated regime in the 2D phase diagram of Fig.2 was established. Note that the scales in computer time needed to achieve convergence are very large near the critical chemical potential where frequent tunneling events between the two minima slow down the simulations. For $J_H/t < 4$, it becomes difficult to distinguish between an actual discontinuity in $\langle n \rangle$ and a very rapid crossover and, thus, in the 2D phase diagram (Fig.2) the boundary of phase separation at small Hund coupling is not sharply defined.

5.3 Incommensurate Correlations

The regime of small coupling J_H/t is not ferromagnetic, according to the behavior of $S(q)$ at zero momentum, and does not correspond to phase separation since all densities are stable. It may occur that robust incommensurate spin correlations exist here, as it occurs in 1D. $S(q)$ is presented in Fig.23 for two representative couplings and a large range of densities. The antiferromagnetic peak at (π, π) is rapidly suppressed as $\langle n \rangle$ decreases, and the position of the maximum in $S(q)$ moves along the (π, π)–$(\pi, 0)$ line (and also along (π, π)–$(0, \pi)$ by symmetry). The intensity of the peak is rapidly reduced as it moves away from (π, π), and the IC character of the correlations is apparently short-range. However, the numerical study of IC phases are notoriously affected by lattice sizes, and thus at

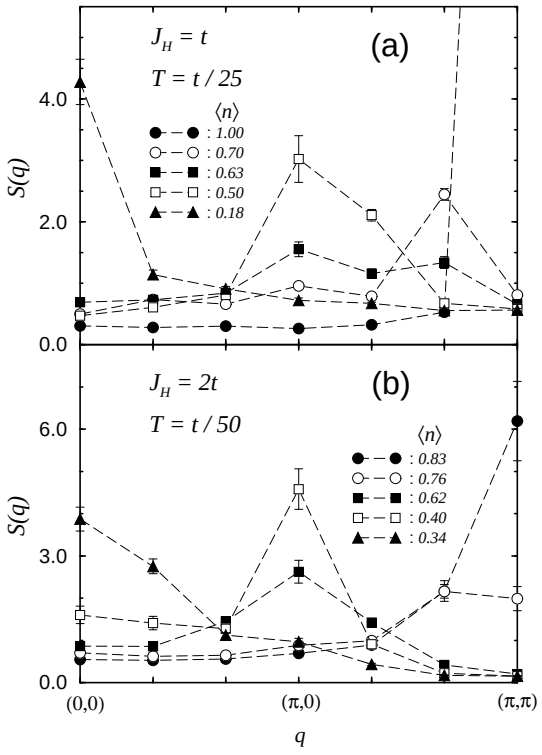

Figure 23: $S(q)$ vs momentum on a 6×6 cluster and at (a) $J_H/t = 1$ and $T = t/25$, and (b) $J_H/t = 2$ and $T = t/50$. In both cases open boundary conditions were used. The densities are indicated.

this stage it can only be claimed that a tendency to form IC spin patterns has been detected in 2D clusters, without a firm statement regarding their short- vs. long-range character. As $\langle n \rangle$ is further reduced, the peak position reaches $(\pi, 0)$ and $(0, \pi)$ with substantial intensity. Reducing further the density, a rapid change into the ferromagnetic phase was observed. At a larger J_H/t coupling such as 3, a more complicated IC pattern was detected with regions where $S(q)$ peaked simultaneously at $(\pi, 0)$-$(0, \pi)$ and $(0, 0)$. Further work is needed to clarify the fine details of the spin arrangements in this regime, but nevertheless the results given here are enough to support the claim that a tendency to form incommensurate correlations exists in the ground state of the 2D FM Kondo model [35].

6 Results in D=∞

The existence of phase separation and ferromagnetism in the ground state of the FM Kondo model can also be studied in the limit of $D = \infty$. The Dynamical Mean Field equation [19] is solved iteratively starting from a random spin configuration, and as a function of temperature and density three solutions have been observed having AF, FM, and paramagnetic character. Efforts were concentrated on a particular large coupling $J_H/W = 4.0$ studying the temperature dependence of the results, where W is the half-width of the semicircular density of states $D(\epsilon) = (2/\pi W)\sqrt{1 - (\epsilon/W)^2}$ for the e_g electrons. Partial results are contained in Fig.24a. The presence of ferromagnetism at finite doping and antiferromagnetism at half-filling are quite clear in the calculations. Close to half-filling and at low temperature, the density $\langle n \rangle$ as a function of μ was found to be discontinuous, in excellent agreement with the results already reported in $D = 1$ and 2. Fig.24b provides a typical example obtained at $T/W = 0.0003$ (results at $T/W = 0.002$ were already presented in Ref. [11]). The phase separation in this figure is between antiferromagnetic and ferromagnetic regions. However, in Fig.24b note that at a slightly larger temperature the separation occurs between hole-poor antiferromagnetic and hole-rich *paramagnetic* regions.

For completeness, in Fig. 25 the density of states $A(\omega)$ for the AF and FM phases is shown at $J_H/W = 2$ and $T/W = 0.005$ (for details of the calculation see Ref.[19]). The critical chemical potential where the AF and FM phases coexist is $\mu_c \sim -1.40W$. $A(\omega)$ in Fig.25 is calculated at $\mu = \mu_c$ for both phases. In the two cases the density of states splits into upper and lower bands due to the large Hund coupling. The width of the upper and lower bands is wider for the FM phase, which causes a narrower gapped region centered at $\omega \sim 0$. Let us now consider the process of hole doping starting at $\langle n \rangle = 1$ and decreasing μ. In the AF phase at $\mu \geq \mu_c$, the chemical potential lies in the gap. However, at $\mu \leq \mu_c$ the chemical potential is located already inside the lower band of the FM phase, since this band is wider than in the AF phase. This suggest that before the lightly doped AF phase is realized in the system by decreasing μ, the FM phase is instead stabilized. Thus, the discontinuous change from the AF to FM phases at $\mu = \mu_c$ also causes a jump in the carrier number. This discontinuity occurs only when the bandwidth of the AF phase is considerably narrower than that of the FM phase. For this reason phase separation exists only in the large J_H region.

Summarizing, at very low temperature there is a remarkable agreement between the $D = \infty$ and $D = 1, 2$ results which were obtained using substantially different numerical techniques. Such an agreement give us confidence that the phase separation effect discussed here is not pathological of low dimensions or induced by approximate algorithms but it is intrinsic of the physics of the FM Kondo model, and likely it exists in dimension $D = 3$ as well.

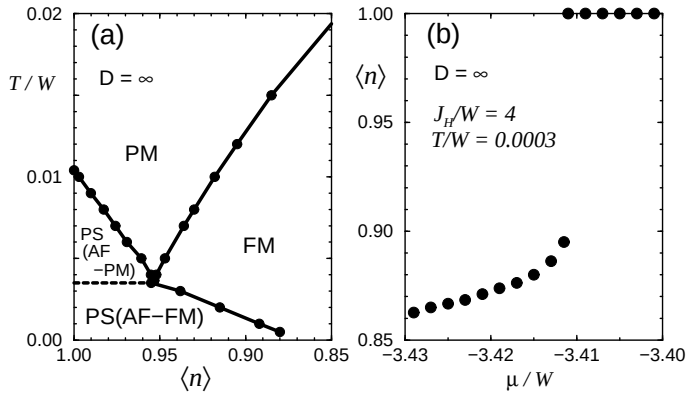

Figure 24: (a) Phase diagram in the $D = \infty$ limit working at $J_H/W = 4.0$. The "PS(AF-PM)" region denotes phase separation (PS) between a hole-poor antiferromagnetic (AF) region, and a hole-rich paramagnetic (PM) region. The rest of the notation is standard; (b) Density $\langle n \rangle$ vs μ/W obtained in the $D = \infty$ limit, $J_H/W = 4.0$, and $T/W = 0.0003$. The discontinuity in the density is clear.

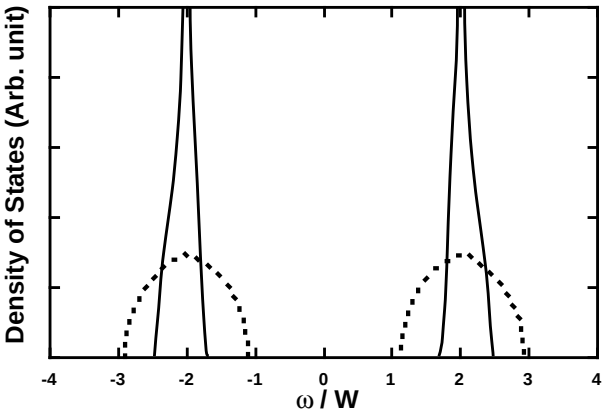

Figure 25: Density of states in the $D = \infty$ limit corresponding to the antiferromagnetic (solid line) and ferromagnetic (dotted line) solutions, working at $J_H/W = 2.0$ and $T/W = 0.005$. The chemical potential is tuned to be at its critical value $\mu_c \sim -1.40W$.

7 Results in D=3

Results in three dimensions for large enough clusters are difficult to obtain with the Monte Carlo algorithm used in this paper. The reason is that the CPU time needed to diagonalize exactly the problem of an electron moving in a fixed spin background grows rapidly with the number of sites. Nevertheless, studies using 4^3 clusters carried out as part of this project have shown clear indications of strong ferromagnetic correlations in a region of parameter space compatible with those found in one and two dimensions where FM dominates, and thus it is reasonable to assume that there are ferromagnetic phases in the FM Kondo model in all dimensions from 1 to ∞. Regarding phase separation, the studies on 4^3 clusters cannot provide conclusive evidence due to the presence of intrinsic gaps in $\langle n \rangle$ vs μ caused by size effects. But once again by simple continuity between $D = 1, 2$ and $D = \infty$, the existence of phase separation in $D = 3$ is strongly suggested by our results.

In spite of the size limitations of studies in three dimensions, it is possible to obtain useful information about the actual value of the critical temperature in the limit of $J_H = \infty$ i.e. working in a region which corresponds to a fully saturated ferromagnetic state at zero temperature. In this limit the problem is simplified since for the mobile electrons only the spin component in the direction of the classical spin survives, as discussed in Sec.II where the effective model ("complex double exchange") was described. The absence of a spin index reduces substantially the CPU time for diagonalization in the numerical algorithm, and allowed us to study clusters with 6^3 sites using the Hamiltonian Eq.(3). Measuring the spin-spin correlation (among the classical spins) in real space and reducing the temperature, it is possible to study at what temperature, T^*, such correlation becomes nonzero at the maximum distance available in a 6^3 cluster. For temperatures higher than T^* the spin correlations can be accommodated inside the cluster and, thus, the ferromagnetic correlation length, ξ^{FM}, is $finite$. Using this idea, upper bounds on the critical temperature can be obtained using $T^* > T_c^{FM}$. In addition, it is reasonable to assume that in a 3D system the growth of ξ^{FM} with T is very rapid once it starts, and T^* itself may actually provide a good estimate of the critical temperature in the bulk.

Figs.26.a-d contain the spin-spin correlations at $J_H = \infty$ on the 6^3 cluster parametric with temperature. Results for four densities are given, and only some representative temperatures are shown. The spin correlations on a 4^3 cluster (not shown) are in good agreement with those provided in Fig.26. Based on this information the temperature where the ferromagnetic correlations reach the boundary with a nonzero value can be obtained with reasonably small error bars. The results are shown in Fig.27a. Once again, assuming a rapid increase of ξ^{FM} as the temperature is reduced, the results of Fig.27a can be considered as a rough estimate of the actual critical temperature. As anticipated in Sec.III.A, T_c^{FM} is maximized at $\langle n \rangle = 0.50$. In Fig.27b, $S(q)$ at zero momentum is presented as a function of temperature for the four densities used in Fig.26. A rapid growth is observed at particular temperatures which are compatible with those obtained in Fig.27a using the tail of the real space correlations. The present results are qualitatively similar to those obtained using high temperature expansions (HTE) [36],

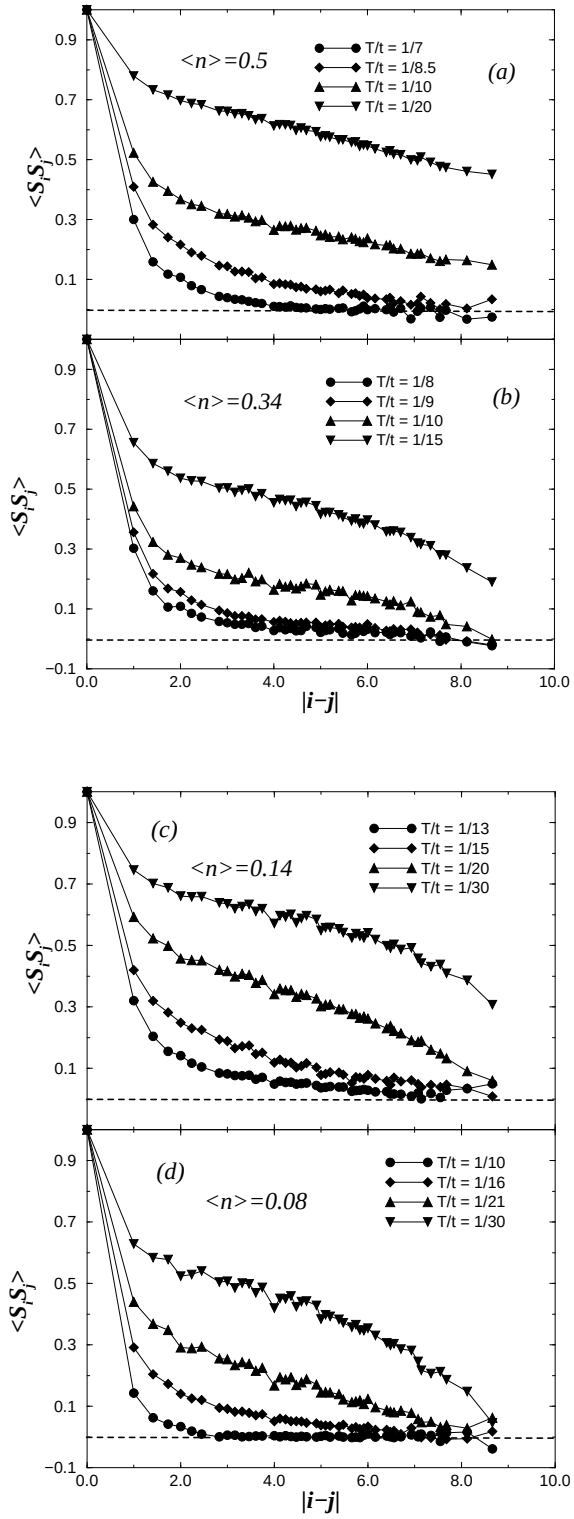

Figure 26: Spin-spin correlations (among the classical spins) vs distance for several temperatures (as indicated) working on a 6^3 cluster and using the Monte Carlo technique. (a) contains results for $\langle n \rangle = 0.50$, (b) for $\langle n \rangle = 0.34$, (c) for $\langle n \rangle = 0.14$, and (d) for $\langle n \rangle = 0.08$.

although our estimates for the critical temperatures are smaller. For instance, at $\langle n \rangle = 0.50$ the HTE prediction gives $T_c^{FM} \sim 0.16t$, about a factor 1.5 larger than our result.

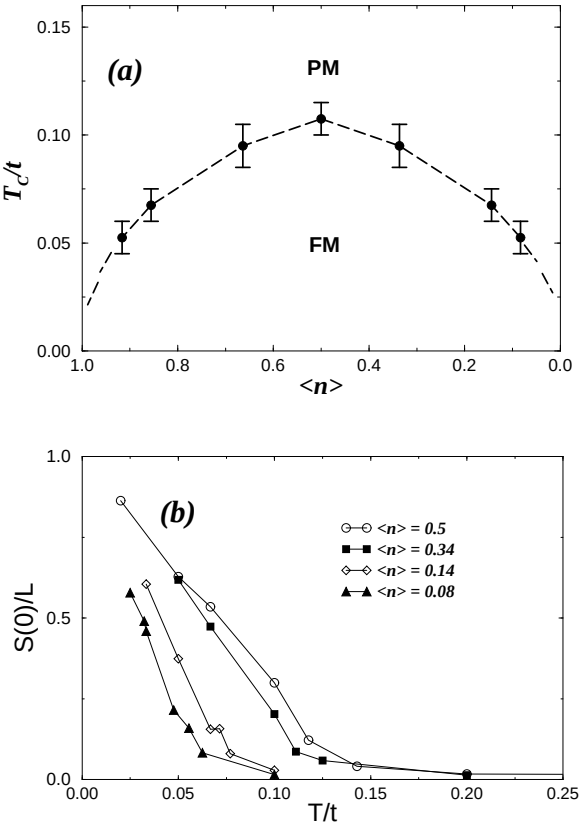

Figure 27: (a) Upper bound for the critical temperature vs density deduced from spin correlations on 6^3 clusters, working at $J_H = \infty$; (b) $S(q = 0)/L$ vs temperature at several densities, obtained with the Monte Carlo method on a 6^3 cluster at $J_H/t = \infty$.

To obtain the critical temperature in degrees, an estimate of t is needed. Results in the experimental literature for the e_g electrons bandwidth range from $BW \sim 1\ eV$ [37] to $BW \sim 4eV$ [38]. Assuming a dispersion $\epsilon_{\mathbf{p}} = -2t(cosp_x + cosp_y + cosp_z)$, the hopping amplitude should be $t = BW/12$ i.e. between 0.08 and 0.33 eV. With this result our estimate for the critical temperature is roughly between $T_c^{FM} \sim 100\ K$ and $400\ K$, which are within the range observed experimentally. Then, in our opinion it is possible to obtain realistic values for T_c^{FM} using purely electronic models, in agreement with other calculations [19, 36].

8 Conclusions

In this paper the phase diagram of the ferromagnetic Kondo model for manganites was investigated. Using a wide variety of computational techniques that include Monte Carlo simulations, Lanczos and DMRG methods, and the Dynamical Mean Field approach, regions in parameter space with (i) robust ferromagnetic correlations, and (ii) phase separation between hole-poor antiferromagnetic and hole-rich ferromagnetic regions were identified. In addition, incommensurate spin correlations were observed in dimension 1 and 2 at small J_H/t. The critical temperature towards ferromagnetism for the case of a three dimensional lattice was also estimated, and the results are compatible with experiments for manganites. The agreement between the results obtained with different computational techniques, working at several spatial dimensions, and using both classical and quantum mechanical localized spins in the case of chains lead us to believe that the conclusions of this paper are robust and they represent the actual physics of the ferromagnetic Kondo model.

The novel regime of phase separation is particularly interesting, and possible consequences of its existence in manganites can be envisioned. Experimentally, phase separation can be detected using neutron diffraction techniques if the two coexisting phases have different lattice parameters as it occurs in $La_2CuO_{4+\delta}$, a Cu-oxide with hole-rich and hole-poor regions [39]. NMR and NQR spectra, as well as magnetic susceptibility measurements, can also be used to detect phase separation [40, 41] since a splitting of the signal appears when there are two different environments for the ions. Note also that in the regime where AF and FM coexist $S(q)$ presents a two peak structure, one located at the AF position and the other at zero momentum. This also occurs in a canted ferromagnetic state and, thus, care must be taken in the analysis of the experimental data. Actually, recent experimental results by Kawano et al. [42] are in qualitative agreement with the results of Fig.24a since these authors observed a reentrant structural phase transition accompanied by "canted ferromagnetism" below T_c^{FM}, at $0.10 < x < 0.17$ in $La_{1-x}Sr_xMnO_3$. In addition the polaron-ordered phase reported by Yamada et al. [43] can be reanalyzed using the results of this paper since it is known that the AF phase in 3D manganites is orthorhombic while the FM is pseudo-cubic. The formation of a lattice superstructure may stabilize the magnetic tendency to phase separate and minimize lattice distortions.

Note, however, that phase separation may manifest itself as in "frustrated phase separation" scenarios [15]: Since the Coulombic interaction between holes was not explicitly included it is possible that in realistic situations phase separation may be replaced by the formation of complex structures, such as the stripes observed in cuprates [16, 17, 18]. Thus, it is reasonable to speculate that these stripes could also appear in the insulating regime of the manganites and they should be detectable using neutron scattering techniques.

On the theoretical side, future work will be directed to the analysis of the influence of phonons and orbital degeneracy into the phase diagram observed in the present paper, specially regarding phase separation, as well as the calculation of dynamical properties for the models investigated here. Work is in progress along these fronts to complete a qualitative understanding of the phase diagram corresponding to models for the manganites beyond the double exchange model.

9 Acknowledgments

We thank K. Hallberg, J. Riera and S. Kivelson for useful conversations. E. D. and A. M. are supported by the NSF grant DMR-9520776. S. Y. is supported by the Japanese Society for the Promotion of Science. J. H. is supported by the Florida State grant E&G 502401002. A. L. M. acknowledges the financial support of the Conselho Nacional de Desenvolvimento Científico e Tecnológico (CNPq-Brazil)

References

[1] S. Jin, et al., Science **264**, 413 (1994), and references therein.

[2] Y. Tokura et al., J. Appl. Phys. **79** (8), 5289 (1996).

[3] G. C. Xiong et al., Appl. Phys. Lett. **66**, 1427 (1995), and references therein.

[4] C. Zener, Phys. Rev. **82**, 403 (1951); P. W. Anderson and H. Hasegawa, Phys. Rev. **100**, 675 (1955).

[5] P. G. de Gennes, Phys. Rev. **118**, 141 (1960).

[6] P. E. Schiffer, A. P. Ramirez, W. Bao, and S-W. Cheong, Phys. Rev. Lett. **75**, 3336 (1995); A. P. Ramirez et al., Phys. Rev. Lett. **76**, 3188 (1996); C. H. Chen and S-W. Cheong, Phys. Rev. Lett. **76**, 4042 (1996). See also H. Y. Hwang, S-W. Cheong, P.G. Radaelli, M. Marezio, and B. Batlogg, Phys. Rev. Lett. **75**, 914 (1995); P. G. Radaelli, D.E. Cox, M. Marezio, and S-W. Cheong, Phys. Rev. **B 55**, 3015 (1997).

[7] A. J. Millis, P. B. Littlewood, and B. I. Shraiman, Phys. Rev. Lett. **74**, 5144 (1995); H. Röder, J. Zang and A. R. Bishop, Phys. Rev. Lett. **76**, 1356 (1996); A. J. Millis, B. Shraiman and R. Mueller, Phys. Rev. Lett. **77**, 175 (1996).

[8] E. Müller-Hartmann and E. Dagotto, Phys. Rev. **B 54**, R6819 (1996).

[9] J. W. Lynn et al., Phys. Rev. Lett. **76**, 4046 (1996).

[10] D. Dessau et al., private communication. See also D. Dessau et al., preprint; and C.-H. Park et al., preprint.

[11] S. Yunoki, J. Hu, A. Malvezzi, A. Moreo, N. Furukawa, and E. Dagotto, preprint cond-mat/9706014.

[12] J. Riera, K. Hallberg and E. Dagotto, Phys. Rev. Lett. **79**, 713 (1997).

[13] V. J. Emery, S. A. Kivelson, and H. Q. Lin, Phys. Rev. Lett. **64**, 475 (1990). Note that in this paper phase separation in the $t-J$ model between hole-rich ferromagnetic and hole-poor antiferromagnetic regions was also proposed. However, in the $t-J$ model the ferromagnetic regions occurs for unphysically small values of J/t, while in the model for manganites studied in the present paper it occurs in a realistic region of parameter space. We thank S. Kivelson for this comment.

[14] E. Dagotto, Rev. Mod. Phys. **66**, 763 (1994); and references therein.

[15] V. J. Emery, and S. A. Kivelson, Physica **C 209**, 597 (1993). In this paper it was proposed that stripes and related structures are a generic feature of doped correlated insulators, in agreement with the results for manganites discussed here. We thank S. Kivelson for this comment.

[16] U. Löw, V. J. Emery, K. Fabricius, and S. A. Kivelson, Phys. Rev. Lett. **72**, 1918 (1994); S. Haas, E. Dagotto, A. Nazarenko, and J. Riera, Phys. Rev. **B 51**, 5989 (1995).

[17] D. Poilblanc and T. M. Rice, Phys. Rev. **B 39**, 9749 (1989).

[18] J. M. Tranquada et al., Nature **375**, 561 (1995), and references therein.

[19] N. Furukawa, J. Phys. Soc. Jpn. **63**, 3214 (1994); *ibid*, 2754 (1995).

[20] For a more technical review on Lanczos methods see D. Poilblanc in "Numerical methods for strongly correlated Systems", Frontiers in Physics, Ed. D.J. Scalapino, Addison-Wesley, Redwood City California (1997).

[21] S. R. White, Phys. Rev. Lett. **69**, 2863 (1992).

[22] K. Kubo, J. Phys. Soc. Jpn. **51**, 782 (1982); J. Zang, H. Röder, A. R. Bishop, and S. A. Trugman, J. Phys.: Condens. Matter **9**, L157 (1997); T. A. Kaplan and S. D. Mahanti, J. Phys.: Condens. Matter **9**, L291 (1997).

[23] Similar results have been recently reported in P. Horsch, J. Jaklič, and F. Mack, preprint cond-mat/9708007.

[24] For a review see J. Voit, Rep. Prog. Phys. **57**, 977 (1994).

[25] J. Inoue and S. Maekawa, Phys.Rev.Lett.**74**, 3407 (1995).

[26] S. Yunoki and A. Moreo, in preparation.

[27] Actually working at very small J_H/t and close to half-filling a ground state singlet was stabilized but it is unclear to what extend this result survives the bulk limit.

[28] B. Batlogg, S-W. Cheong, and L. W. Rupp, Jr., Physica (Amsterdam) **194 - 196B**, 173 (1994); A. P. Ramirez et al., Phys. Rev. Lett. **72**, 3108 (1994); J. F. DiTusa, et al., Phys. Rev. Lett. **73**, 1857 (1994).

[29] E. Dagotto, J. Riera, A. Sandvik and A. Moreo, Phys. Rev. Lett. **76**, 1731 (1996).

[30] The $S=1$ chain has a nonzero Haldane gap at half-filling. However, a low density of holes closes the gap as recently observed numerically [29]. Then, a "spin-gap" regime is not included in the phase diagram of the model with localized $S=1/2$ spins.

[31] E. Dagotto, A. Moreo, F. Ortolani, D. Poilblanc, and J. Riera, Phys. Rev. **B 45**, 10741 (1992).

[32] Nevertheless it was observed that the ground state energy vs density is almost linear in the range corresponding to 0, 2 and 4 holes, and thus phase separation may appear if larger clusters could be studied.

[33] Note that a trivial factor 2 in the overall J_H scale can be accounted for by considering that the mobile spin in Eq.(8) is 1/2, while in Sec.IV.B for the conduction electrons no factor 1/2 was used in the Hund term.

[34] Y. Moritomo, A. Asamitsu, H. Kuwahara, Y. Tokura, Nature **380**, 141 (1996).

[35] Our results for the IC correlations in 2D are in qualitative agreement with M. Hamada and H. Shimahara, Phys. Rev. **B 51**, 3027 (1995).

[36] H. Röder, R. R. P. Singh, and J. Zang, preprint.

[37] Y. Moritomo, A. Asamitsu and Y. Tokura, Phys. Rev. **B 51**, 16491 (1995).

[38] D. D. Sarma et al., Phys. Rev. **B 53**, 6873 (1996).

[39] P. G. Radaelli, J. D. Jorgensen, R. Kleb, B. A. Hunter, F. C. Chou, and D. C. Johnston, Phys. Rev. **B 49**, 6239 (1994) and references therein.

[40] P. C. Hammel, A. P. Reyes, S-W. Cheong, Z. Fisk, and J. E. Schirber, Phys. Rev. Lett. **71**, 440 (1993), and references therein.

[41] It is interesting to observe that experimental studies of $Sr_{2-y}La_yMnO_4$ have reported evidence for electronic phase separation and charge ordering at small y. See W. Bao, et al., preprint. See also J. Q. Li et al., Phys. Rev. Lett. **79**, 297 (1997) for phase segregation in $La_{1-x}Sr_xFeO_3$.

[42] H. Kawano et al., Phys. Rev. **B 53**, R14709 (1996); Phys. Rev. **B 53**, 2202 (1996).

[43] Y. Yamada et al., Phys. Rev. Lett. **77**, 904 (1996).